NIH Public Access
Author Manuscript
Biomaterials. Author manuscript; available in PMC 2014 January 01.

Published in final edited form as:
Biomaterials. 2013 January ; 34(2): 552–561. doi:10.1016/j.biomaterials.2012.09.065.

Blood-Stable, Tumor-Adaptable Disulfide Bonded mPEG-$(Cys)_4$-PDLLA Micelles for Chemotherapy

Seung-Young Lee[1], **Sungwon Kim**[2], **Jacqueline Tyler**[1], **Kinam Park**[1,2,*], and **Ji-Xin Cheng**[1,3,*]

[1]Weldon School of Biomedical Engineering, Purdue University, West Lafayette, IN 47907

[2]Department of Industrial and Physical Pharmacy, Purdue University, West Lafayette, IN 47907

[3]Department of Chemistry, Purdue University, West Lafayette, IN 47907

Abstract

Although targeted delivery mediated by ligand modified or tumor microenvironment sensitive nanocarriers has been extensively pursued for cancer chemotherapy, the efficiency is still limited by premature drug release after systemic administration. Herein we report a highly blood-stable, tumor-adaptable drug carrier made of disulfide (DS) bonded mPEG-$(Cys)_4$-PDLLA micelles. Intravenously injected disulfide bonded micelles stably retained doxorubicin in the bloodstream and efficiently delivered the drug to a tumor, with a 7-fold increase of the drug in the tumor and 1.9-fold decrease in the heart, as compared with self-assembled (SA), non-crosslinked mPEG-PDLLA micelles. *In vivo* administration of disulfide bonded micelles led to doxorubicin accumulation in cancer cell nuclei, which was not observed after administration of self-assembled micelles. With a doxorubicin dose as low as 2 mg/kg, disulfide bonded micelles almost completely suppressed tumor growth in mice.

I) Introduction

Targeted delivery using nanocarriers has been studied for several decades with the goal of overcoming rapid clearance and non-specific toxicity of free drugs [1–3]. To date, size-controlled [4], ligand-mediated [5], and microenvironment-responsive [6] nanocarriers have been developed to achieve targeted drug delivery. However, only a few of these carriers are in clinical trials, and even the commercialized nanotherapeutics (e.g., Doxil® and Abraxane®) are unable to completely prevent tumor regrowth or relapse after the treatment [7–9]. Therefore, it is necessary to revisit nanocarrier-based delivery strategy and rethink the key factors in the design of nanocarriers [10, 11].

As one of the representative nanocarriers, polymeric micelles have been widely used in cancer chemotherapy, owing to their high drug loading capacity and readily modifiable chemical structure [12, 13]. Amphiphilic block copolymers, composed of hydrophobic and hydrophilic chain blocks, self-assemble into micelle structure in aqueous solution [14].

© 2012 Elsevier Ltd. All rights reserved.

*Corresponding authors: jcheng@purdue.edu; kpark@purdue.edu.

Publisher's Disclaimer: This is a PDF file of an unedited manuscript that has been accepted for publication. As a service to our customers we are providing this early version of the manuscript. The manuscript will undergo copyediting, typesetting, and review of the resulting proof before it is published in its final citable form. Please note that during the production process errors may be discovered which could affect the content, and all legal disclaimers that apply to the journal pertain.

Appendix A. Supplementary information
Detailed methods can be found in the Supplementary Information.

$watermark-text
$watermark-text
$watermark-text

$watermark-text

$watermark-text

$watermark-text

Hydrophobic anticancer drug can be readily encapsulated inside of the micelle core, and a protective shell, such as a poly(ethylene glycol) (PEG) layer, can be used to shield the micelle from plasma protein opsonization [15]. Anticancer drug-loaded micelles have demonstrated a high tumor accumulation efficiency via the enhanced permeability and retention (EPR) effect, which results from the abnormalities of tumor blood and lymphatic vasculature [16]. However, recent studies have shown that self-assembled polymeric micelles lose their drug content immediately after systemic administration, mainly due to structural dissociation by blood components [17–19]. Thus, one of the most important "prerequisites" in the design of an efficient drug carrier is to stably retain the loaded drug in blood circulation before accessing cancer cells [20]. Another important factor is reduction of non-specific toxicity to healthy organs [21]. Without satisfying these requirements, targeted drug delivery strategies will have difficulty reaching the next level of clinical relevance.

We increase chemotherapeutic efficacy through the design and synthesis of blood-stable, tumor-adaptable micelles, by introducing disulfide bonds at the interface between the hydrophobic core and hydrophilic shell. The disulfide bond was selected due to the strength of its chemical bond (bond energy of ~ 60 kcal mol^{-1}), and its ability to cleave under reductive conditions [22, 23]. Inside the body, glutathione (GSH), a natural reducing agent of disulfide bonds, is known to have a substantially higher concentration (1~10 mM) in cytoplasm than in extracellular fluid (1 ~ 10 μM) [24, 25]. Moreover, the GSH concentration in some cancers was found to be about seven times higher than that in normal cells [26, 27], possibly because GSH metabolism is not only associated with cancer development, but also with drug resistance [28]. We synthesized disulfide (DS) bonded methoxypoly(ethylene glycol)-$(Cysteine)_4$-poly(D,L-lactic acid) (mPEG-$(Cys)_4$-PDLLA) micelle, and via fluorescence resonance energy transfer (FRET) imaging, we characterized *in vivo* blood-stability and tumor-adaptability of disulfide (DS) bonded micelles as compared to self-assembled (SA), non-crosslinked mPEG-PDLLA micelles. Additionally, the anti-tumor activity of doxorubicin-loaded DS micelles in a M109 tumor xenograft mouse model was also investigated.

II) Materials and Methods

i) Polymer synthesis and micelle preparation

Details on the synthesis of copolymers and their fluorescent conjugates can be found in the Supplementary Information. mPEG-PDLLA (SA) and mPEG-$(Cys)_4$-PDLLA (DS) micelles withDiO and DiI were prepared using the membrane dialysis method. Briefly, copolymers were dissolved in DMSO with DiO and DiI. After stirring for 30 min, the solution was repetitively dialyzed (MWCO3500) against degassed MES buffer (1 mM, pH 5.0), distilled degassed water, Tris buffer (1 mM, pH 8.5) with 0.1% (v/v) hydrogen peroxide, and distilled water in sequence for 4 days. The resulting solution was lyophilized. Doxorubicin (DOX) also was loaded in SA and DS micelles using a solvent evaporation method. Neutralized DOX by TEA in chloroform was added to the polymer solution in Tris buffer (1 mM, pH 5.7) while stirring. Using vacuum-evaporation of chloroform, DOX was encapsulated in the micelles. Untrapped DOX and TEA were removed by dialysis (MWCO 3500), and the solution was lyophilized.

ii) *In vitro* stability tests

The fluorescence spectra of SA and DS FRET micelles at 200 μg/ml in various solvents were measured with excitation at 475 nm and emission scanning from 490 nm to 590 nm during incubation at 25°C or 37°C. The FRET ratio was calculated as follows:

$$\text{FRET ratio} = I_{DiI}/(I_{DiI}+I_{DiO})$$

where I_{DiI} and I_{DiO} were the fluorescence intensities of DiI at 570 nm and DiO at 508 nm.

The fluorescence spectra of DOX-loaded SA and DS micelles (containing the same concentration of DOX at 20 μg/ml) in various solvent conditions were measured at 470 nm excitation, and emission scanning from 520 nm to 700 nm during incubation at 25°C or 37°C. The recovery of DOX fluorescence was determined as follows:

$$\text{Recovery percentage (\%) of DOX fluorescence} = ((F\text{-}F_W)/F_D) \times 100$$

where F_W and F_D were the integrated fluorescence emissions in water and DMSO with 100 mM DTT.

iii) Mouse tumor models

All protocols for this animal study were approved by the Purdue Animal Care and Use Committee. M109 (2×10^6) cells were subcutaneously injected in 6-week-old male BALB/c mice.

iv) Real-time FRET imaging of blood vessels

SA or DS FRET micelles (500 μg/100μl in PBS (pH 7.4)) were intravenously injected through the tail vein of a mouse. FRET imaging of blood vessels in the mouse's ear was carried out using a FV1000 confocal system (Olympus, Tokyo, Japan) equipped with a 40× water objective (working distance: 3.3 mm) under inhalation anesthesia. FRET images were acquired with 488 nm excitation and spectral filters of 500–530 nm and 555–655 nm for DiO and DiI detection. Microspectroscopy at the pixels of a blood vessel was conducted using a spectral detector, with emission scanning from 490 nm to 590 nm. To remove signal variations caused by different vessel depths, the fluorescence intensities were rescaled into the same range for easy comparison of the spectral profiles.

v) FRET imaging of tissues

DS FRET micelles (1 mg/200μl in PBS (pH 7.4)) were intravenously injected through the tail vein of a M109 tumor-bearing mouse. After 6 h, the mouse was sacrificed, and tissues were harvested. The tissues then were cross-sectioned using a vibration microtome without fixation. FRET imaging of sectioned tissues followed the same method using a FV1000 confocal system as described above.

vi) Plasma pharmacokinetics

To determine pharmacokinetics, either DOX·HCl (at 4 mg/kg, 200 μl), DOX/SA micelle or DOX/DS micelle (at 4 mg DOX Equiv/kg, 200 μl) was intravenously injected into BALB/c mice through the tail vein using a catheter. A blood sample (2 μl) was collected from the tail vein at different time points post injection and mixed with K3-EDTA (0.5μl, an anticoagulation agent) containing DTT (final concentration: 100 mM, a reducing agent). To extract DOX, acetone (6 μl) was added to the blood, vortexed, and then the solution was centrifuged (5,000×g, 10 min). Fluorescence was measured using a microplate reader with excitation at 470 nm and emission at 590 nm. A linear standard curve of DOX ranging 6.25 – 0.1 μg/ml was created and used for measuring the concentration of DOX in blood.

vii) Tissue biodistribution

DOX·HCl (at 4 mg/kg, 200 μl), DOX/SA(-Cy5.5), and DOX/DS(-Cy5.5) micelles (at 4 mg DOX Equiv/kg, with similar absorption intensity of Cy5.5, 200 μl) were intravenously injected into M109 tumor bearing mice. At 1 day after injection, the mice were sacrificed by transcardial perfusion with 10 mM PBS (pH 7.4) and the tissues and urine were harvested. Cy5.5 in the specimen was imaged by IVIS Lumina (Caliper Life Sciences, Inc., MA) with

$watermark-text $watermark-text $watermark-text

excitation at 640 nm and emission at 695–770 nm. Quantitative analysis for the tissue distribution of micelles was carried out using Living Imaging Software (Caliper Life Sciences, Inc., MA). The tissues were then weighed and homogenized using a tissue grinder. To extract DOX, the tissue solution (50 μl) was mixed with acetone (150 μl) containing DTT (final concentration: 100 mM), and then the solution was centrifuged (5,000×g, 10 min). Fluorescence of the supernatant was measured using a microplate reader with excitation at 470 nm and emission at 590 nm. After subtracting the auto-fluorescence, using the tissues in non-treated mice group, the concentrations of DOX in tissues were quantitatively determined based on the calibration curve of DOX in blood.

viii)Antitumor effects

After reaching a tumor volume of ~30 mm^2, the tumor (M109)-bearing mice were randomized into four groups. The mice received PBS (200 μl), DOX·HCl (at 2 mg/kg, 200 μl), DOX/SA, or DOX/DS micelles (at 2 mg DOX Equiv/kg, 200 μl) through tail vein injection at day 0 and 4 post initial treatment. Tumor volume was measured as follows:

$$V = (a \times b^2) / 2$$

where a and b represent the major and minor axes of a tumor, respectively. The lengths of the axes were measured using a caliper. Tumor volume in each group was compared by relative tumor volume:

$$\text{Relative tumor volume} = \text{tumor volume} / \text{initial tumor volume before treatment}$$

ix) Statistical analysis

Values are expressed as mean ± SEM, and statistical comparisons between groups were made using the Student's t-test and a P value of <0.05 was considered significant.

III) Results

i) Development and *in vitro* characterization of DS micelles

Disulfide cross-linkable block copolymer, methoxypoly(ethylene glycol)-$(Cysteine)_4$-poly(D,L-lactic acid) (mPEG-$(Cys)_4$-PDLLA) was synthesized by incorporating oligo-$cysteine_4$ (C-C-C-C) into the inter-location between the mPEG and PDLLA blocks. This configuration maintains the protective function of PEG shell, and also permits stable encapsulation of a hydrophobic anticancer drug into the micelle core. We also prepared mPEG-PDLLA di-block copolymer as a control. Successful synthesis of the mPEG-$(Cys)_4$-PDLLA copolymer was confirmed by ^1H NMR spectroscopy and GPC measurements (Supplementary Fig. S1). As depicted in Fig. 1a, two different FRET micelles were prepared by physically loading a hydrophobic FRET pair (DiO and DiI) into the cores of both self-assembled (SA) and disulfide (DS) bonded micelles. Physiochemical characteristics of the FRET micelles were analyzed (Table S1). To validate the FRET micelles, fluorescence spectra of SA and DS micelles in deionized water and 80 % (v/v) DMSO were measured (Supplementary Fig. S2). For intact SA micelles in deionized water, the emission was dominated by the peak of DiI at 570 nm, with excitation of DiO at 475 nm. This spectral profile is due to the inter-molecular energy transfer between adjacent DiO and DiI in the micelle core [18, 29]. By adding DMSO, however, the emission peak of DiO at 508 nm increased dramatically, whereas the fluorescence intensity at 570 nm diminished. This is the result of the increasing distance between DiO and DiI due to structural dissociation of the SA micelles. Accordingly, the FRET ratio $I_{DiI}/(I_{DiI}+I_{DiO})$ decreased from 0.92 to 0.26. In contrast, only a modest change in the fluorescence spectrum of DS micelles was observed after adding DMSO, with a decrease in the FRET ratio from 0.92 to 0.72. By placing the DS micelles in 100 % (v/v) DMSO, however, the FRET ratio dropped to 0.26 due to the

$watermark-text $watermark-text $watermark-text

$watermark-text

$watermark-text

$watermark-text

extraction of the probes from the DS micelle core by pure organic solvent. Nevertheless, DS micelles can maintain structural integrity better than SA micelles under organic solvent conditions. These results show that release of core-loaded molecules and structural decomposition can be monitored using FRET micelles.

To examine the stability of micelles under physiological conditions, SA and DS micelles were suspended in 80 % FBS solution and incubated at 37 ºC. The fluorescence spectra were then measured at different incubation times (Fig. 1b). In the SA micelle spectra, the DiO signal at 508 nm increased extensively during the 120 min incubation period, whereas a huge decrease in the DiI intensity at 570 nm was found during the first 30 min, followed by small increase in the intensity with the maximum peak wavelength shifting from 570 to 565 nm. The initial drop in the intensity at 570 nm is likely due to burst release of the probes located at the interface between the hydrophobic and hydrophilic compositions in the micelles [30, 31]. Also, the release of self-quenched DiI in the micelle core can cause not only an increase in the intensity of the signal, but also a decrease in the maximum peak wavelength at the following stage [32]. In contrast, DS micelles showed negligible changes in the time-course spectra, other than the initial drop of DiI intensity at 570 nm after 30 min of incubation. However, the time-resolved spectrum of DS micelles in serum was dramatically altered through incubation with 10 mM GSH, in which case the spectrum profile became similar to that of SA micelles in serum. The time-resolved spectra were re-organized to show the FRET ratio as a function of incubation time (Fig. 1b, right). During the incubation period, the FRET ratio $I_{DiI}/(I_{DiI}+I_{DiO})$ of the SA micelles rapidly decreased from 0.95 to 0.63 due to structural dissociation by serum proteins such as globulines [18], whereas the FRET ratio of the DS micelles in serum gradually reduced from 0.91 to 0.83. However, while incubating with GSH, the FRET ratio greatly dropped from 0.89 to 0.55, reflecting the release of hydrophobic probes from DS micelles mediated by cleavage of disulfide bonds. These results collectively show that DS micelles are not only stable in serum, but are also degradable by GSH.

We further tested the stability and reducibility of doxorubicin (DOX)-loaded micelles, utilizing the self-quenching property of DOX fluorescence. Excess DOX encapsulated in the micelle core triggers the self-quenching of DOX fluorescence, which can be used to investigate the structural changes undergone by the micelles [33, 34]. The characteristics of DOX-loaded micelles were detailed in Table S1. The fluorescent intensities of DOX/SA and DOX/DS micelles in DMSO with 100 mM DTT were remarkably higher than those in water (Supplementary Fig. S3). In time-lapse spectra of DOX-loaded micelles in serum, the fluorescence intensity of DOX/SA micelles significantly increased during the incubation period, while only a modest intensity change in the DOX/DS micelles was observed (Fig. 1c). However, through incubation with 10 mM GSH, the fluorescence intensity of DOX/DS micelles was extensively elevated. These time-resolved spectra were re-organized as a function of percent recovery of DOX fluorescence (Fig. 1c, right). After 9 h of incubation, there was a higher recovery observed for DOX fluorescence intensity of SA micelles (27%) compared to that of the DS micelles (13%), indicating a fast release of DOX by structural disintegration of the SA micelles in serum. Incubation with 10 mM GSH increased the recovery of DOX fluorescence intensity of DS micelles up to (20%), corresponding to cleavage of the disulfide bonds. These results show that the introduction of disulfide bonds significantly improved the stability of polymeric micelles, and thus efficiently retained anticancer drugs encapsulated in the micelle core under physiological conditions. Furthermore, under subcellular reducing conditions (GSH ~ 10 mM) [24], the disulfide bonds can be reduced, allowing the release of anticancer drugs from DS micelles.

$watermark-text

$watermark-text

$watermark-text

ii) Stability of DS micelles during circulation

We next evaluated the stability of the micelles in blood circulation using *in vivo* real-time FRET imaging. SA or DS micelles were intravenously injected into mice through the tail vein, followed by FRET imaging of the blood vessels in the ear lobes (Fig. 2a,b). At 15 min after injection of SA micelles, we observed not only the strong signal of DiO (green) but also the distinct fluorescence signals of both DiO (green) and DiI (red) on the blood vessel walls. In contrast, for DS micelles, only the signal of DiI (red) in the blood vessels was captured at the initial time point and there was no detectable fluorescence signal on the blood vessel walls. The spectra clearly showed signal changes during blood circulation (Fig. 2a,b, right). The FRET ratio $I_{DiI}/(I_{DiI}+I_{DiO})$ of SA micelles in bloodstream rapidly decreased from 0.58 at 15 min-post injection to 0.51 at 1 h, 0.42 at 6 h, and 0.38 at 12 h. In contrast, the FRET ratio of DS micelles slowly reduced from 0.84 at 15 min-post injection to 0.77 at 1h, 0.58 at 6 h, and 0.54 at 12 h. The low level of plasma GSH may have caused the sustained release of the hydrophobic dyes from the DS micelle core. Comparing the data above with the ratios of the micelles in water (0.92) and DMSO (0.26), SA micelles only retained less than half of the FRET efficiency at 15 min after injection, and had nearly complete loss of FRET at 12 h. On the other hand, DS micelles preserved higher FRET efficiency during the blood circulation time. This is consistent with the *in vitro* FRET results, in which DS micelles in serum maintained higher FRET ratios over the incubation time.

Furthermore, apparent fluorescence on the blood vessel walls indicates that DiO and DiI had been liberated from the SA micelles in the bloodstream, and were incorporated into the endothelial cell membranes. Lipophilic carbocyanine dyes, such as DiO and DiI, have been widely used to label the cell membrane [35] and visualize blood vessels [36], owing to the direct interaction of their hydrocarbon chains and the membrane lipid bilayer [37]. DiO and DiI, which were encapsulated in the DS micelle core, however, could not contact the endothelial cell membrane, resulting in no fluorescent signal on the blood vessel wall. These results suggest that DS micelles can stably retain payloads in blood circulation, whereas SA micelles immediately lose their payloads after systemic administration.

iii) Tumor-adaptability of DS micelles

The adaptability of DS micelles for the treatment of tumors was investigated by FRET imaging. At 6 h after the injection of DS micelles to M109 tumor-bearing mice, the main organs were harvested and sectioned, after which confocal FRET images were acquired. In the tumor tissue, the signal of DiI (red) was predominant in the tumor blood vessels, while a strong overlaid signal (yellow) of DiO (green) and DiI (red) was apparent in the cancer cells (Fig. 3a). The high-magnification images clearly displayed the fluorescent signals of both DiO and DiI in a single cell. These observations are further evidenced by the spectra in the blood vessel and cancer cells (Fig. 3b). The FRET ratios in the blood vessel and cancer cell were 0.66 and 0.31, respectively. This data implicates the different structural responses of DS micelles to the different micro-environments in the blood and cancer cell. Considering GSH content, cancer cells have a significantly higher concentration of GSH than the extracellular fluids [24, 26]. Therefore, it is probable that injected DS micelles stably circulated in blood, reached the tumor via extravasation, were internalized by cancer cells, and were then dissociated in the cells by intracellular GSH. In the FRET images of other tissues, the red fluorescence (DiI) was primarily observed, though weak yellow fluorescence was observed in the spleen and kidney, which is likely due to the disintegration of some DS micelles by splenic macrophages and glomerular filtration (Fig. 3c). This result further shows that DS micelles remain stabilized through the reticuloendothelial system (RES) such as the liver and spleen, in which immune cells localize to eliminate exogenous organisms [38].

$watermark-text

$watermark-text

$watermark-text

iv) Pharmacokinetics and tissue-distribution of DOX/DS micelles

To measure the retention time of anticancer drug in blood via micelle-mediated delivery, DOX·HCl, DOX/SA, and DOX/DS micelles were systemically injected to mice at the same dose of 4 mg/kg DOX and the plasma DOX concentration was measured as a function of time postinjection. One- or two-compartment pharmacokinetic model was used to fit the plasma concentration-time profiles (Fig. 4a). Pharmacokinetic values also were calculated based on these models (Table S2). The DS micelle-mediated delivery extended the plasma half-life of DOX to ~11.6 h as compared with DOX·HCl (~0.05 h). Furthermore, the plasma AUC of DOX for DOX/DS micelles (~92) was significantly larger than those for DOX·HCl (~0.52) and DOX/SA micelles (~40). The results show that DS micelles can extensively prolong the retention time of doxorubicin in blood.

To characterize tissue distributions of DOX and the micelles, we synthesized DOX-loaded, Cy5.5-labeled SA and DS micelles (DOX/SA(-Cy5.5) and DOX/DS(-Cy5.5) micelles). Colocalization of fluorescence signals from DOX (red) and Cy5.5 (cyan blue) evidenced the encapsulation of DOX into the micelles (Supplementary Fig. S4). DOX·HCl, DOX/SA(-Cy5.5), and DOX/DS(-Cy5.5) micelles at the same DOX dose (4 mg/kg) were intravenously injected into M109 tumor-bearing mice. The tissue distribution of DOX at 1 day-post injection was spectrophotometrically determined after transcardial perfusion (Fig. 4b). Importantly, the DS micelles delivered DOX to the tumor with around 19 and 7-fold higher concentration than DOX·HCl and DOX/SA micelle groups, respectively. Most DOX delivered by DOX·HCl or SA micelles was found in urine as a result of renal clearance. Equally important, the DS micelles reduced the concentration of DOX in heart by 1.5 and 1.9-fold as compared to the DOX·HCl and DOX/SA micelles ($P < 0.001$). This indicates that the use of DS micelle as a DOX carrier can minimize the possibility of DOX-associated side effects in the heart, such as cardiomyopathy and congestive heart failure [39]. This result also suggests that the maximum tolerated dose (MTD) of DOX can be increased through DS micelle-mediated delivery [40].

The tissue distribution of the micelles at 1 day-post injection was determined using near-infrared fluorescence (NIRF) imaging of Cy5.5 linked to the micelles, and the fluorescence intensity was quantitatively analyzed (Fig. 4c,d). A strong signal for both SA and DS micelles was observed in the kidney, and we confirmed Cy5.5 fluorescence in the urine sample, reflecting renal clearance of the micelles. Notably, a higher intensity of SA micelles in the liver was measured as compared to DS micelles, implicating that the liver readily captured SA micelles, which had separated with DOX during blood circulation. In addition, the fluorescence intensity of DS micelles in the tumor was around 2-fold higher than that of the SA micelles. Together, these findings demonstrate that stable DS micelles in the blood circulation can not only substantially increase the tumor-target efficacy of DOX, but they can also decrease the possibility of side effects in the heart.

v) Antitumor activity of DOX/DS micelles

The antitumor activity of the micelles against subcutaneous M109 tumors was evaluated in Fig. 5. DOX·HCl, DOX/SA, and DOX/DS micelles with the same DOX dose of 2 mg/kg were systematically administrated at day 0 and 4. Although *in vitro* cytotoxicity testing didn't show any differences in antitumor activities (Supplementary Fig. S5), only DOX/DS micelles significantly inhibited tumor growth *in vivo*, whereas DOX·HCl and DOX/SA micelles failed to prevent tumor growth. Moreover, no significant difference in antitumor activities was found between PBS, DOX·HCl, and DOX/SA micelles ($P > 0.1$). This is likely due to the low doses of DOX (2 mg/kg), as compared with the dose of 8~10 mg/kg used for the treatment of M109 tumors in previous reports [41, 42]. Despite the low DOX dosage, our DS micelles demonstrated high antitumor activity. Histochemical examination

of tumor tissues demonstrated that only the tumor treated with DOX/DS micelles had a strong TUNEL signal (green fluorescence), indicating a significant presence of apoptotic cells (Fig. 5c). This data highlights the promising potency of DS micelles as a drug carrier for cancer chemotherapy.

vi) Intracellular DOX delivery mediated by DS micelles

To further understand the higher chemotherapeutic efficiency of DS micelles, we assessed intracellular drug delivery in mice using DS and SA micelles. Confocal fluorescence images of tumor tissue harvested at 12 h-post injection of DOX/SA(-Cy5.5) and DOX/DS(-Cy5.5) micelles are shown in Fig. 6. No fluorescence signals from DOX and Cy5.5 for DOX/SA micelle were observed, while the distinct fluorescence of DOX (red) and Cy5.5 (cyan blue) in blood vessels and cancer cells for DOX/DS micelle were exhibited. Notably, the distribution image of DOX/DS micelles at a single cell level clearly revealed the colocalization of DOX (red) and the nucleus (green), and the existence of DS micelles (Cy5.5, cyan blue) in the cytoplasm. Markedly, the *in vitro* cellular uptake study showed no significant difference in intracellular DOX delivery between SA and DS micelles (Supplementary Fig. S6). These results collectively demonstrate that DS micelles are able to successfully deliver anticancer drugs to intracellular target organelle *in vivo*.

IV)Discussion

Two great challenges associated with targeted drug delivery in cancer chemotherapy are low efficiency of drug delivery to tumor, and non-specific toxicity to healthy organs. Over the past decade, various functionalized nanocarriers have been developed, such as tumor microenvironment-sensitive (e.g. pH [43] and ions [44]_ENREF_46) and targeting ligand-conjugated nanocarriers [45]. However, without the guarantee of stability under physiological conditions, such nanocarriers could not overcome these challenges. Recently, a clinically relevant strategy to enhance the stability of nanocarriers through formation of disulfide bonds was introduced. Koo *et al.* reported that disulfide cross-linked poly(ethylene glycol)-b-poly(Llysine)-b-poly(L-phenylalanine) (PEG-PLys-PPhe) micelles showed prolonged circulation time in blood, and enhanced the therapeutic efficacy of docetaxel (DTX) in MDA-MB231 tumor-bearing mice as compared with original PEG-PLys-PPhe micelles [46]. Li *et al.* prepared disulfide cross-linked micelles (DCMs) that demonstrated a long retention time in blood, less hemolytic activities, and superior accumulation in SKOV-3 tumor as compared to non-cross-linked micelles (NCMs) [47]. In spite of these initial studies, crucial questions remained unanswered: (*i*) Can the carriers stably encapsulate drugs during blood circulation? (*ii*) Although the carriers themselves showed higher blood retention and tumor targeting, can the carriers improve the pharmacokinetics and tumor-target efficacy of drugs? (*iii*) Do the carriers respond to tumor and cancer cells after reaching the cells by the blood circulation and extravasation? (*iv*) Can the carriers deliver an anticancer drug to subcellular target organelle?

A major obstacle for elucidating these questions was the absence of appropriate techniques to investigate whether the nanocarriers remained intact after systemic administration. Imaging of fluorescently labeled nanocarriers can provide information on pharmacokinetics and biodistribution of the nanocarriers, but in using this method it is not obvious whether the fluorescent signals come from the intact nanocarriers. Therefore, there is no evidence that the anticancer drug was reasonably delivered to the tumor following the original hypothesis of nanocarrier-based delivery. Kazunori Kataoka and his group used the self-quenching of a core conjugated fluorophore to assess the intactness of poly(ethylene glycol)-b-poly(glutamic acid) (PEG-bP(Glu)) micelles [44]. Their method requires additional chemical conjugation of a fluorophore, and hence may affect the physiochemical properties of the original micelles. Furthermore, the previous method, which relies on the intensity

$watermark-text $watermark-text $watermark-text

$watermark-text

$watermark-text

$watermark-text

change at a wavelength, is limited in its ability to characterize the intactness of nanocarriers at different tissue depths, due to depth-dependent attenuation of fluorescence intensity.

In this paper, we physically loaded hydrophobic FRET probes to the micelle core. This method allowed us to spatiotemporally monitor the intactness of nanocarriers at different depths in blood vessels and tissues without additional chemical conjugation and normalization processes. Through FRET imaging, we clearly answered the questions raised above by showing that disulfide (DS) bonded micelles could (*i*) stably retain anticancer drugs in bloodstream, (*ii*) improve the blood-retention and tumor-target efficiency of anticancer drugs, (*iii*) structurally respond to tumor micro-environments, and (*iv*) deliver anticancer drugs to intracellular target organelle. These results highlight the utilization of FRET techniques for the structural characterization of nanocarriers.

It is important to compare our approach with other approaches in which drug delivery is mediated by a tumor-targeting ligand. Our study showed that reinforced stability of micelles in physiological conditions by disulfide bonding led to a 7-fold increase in DOX delivery to tumor, compared to SA micelles, without any additional modification such as ligand conjugation. Although various targeting ligands for cancer therapy have been applied to tumor-targeting drug delivery [48], the enhancement of nanocarrier accumulation in tumors by the inclusion of targeting ligands is still a controversial issue. Several recent reports have shown only modest improvement in tumor accumulation using liganded nanocarriers as compared to nanocarriers without ligands [49, 50]. These results may be attributed to instability of the nanocarriers in physiological conditions, but not the bioavailability of the targeting ligands. Collectively, our data indicates that the stability of nanocarriers is the primary factor to be considered in targeted drug delivery. It is anticipated that ligand conjugation to stable DS micelles can further increase specific tumor-targeted delivery and therapeutic efficacy of anticancer drugs.

V) Conclusions

We have shown that our disulfide (DS) bonded micelles possess high stability in blood circulation and tumor-adaptability. These complementary properties significantly improved the retention time of DOX in blood and the target efficacy of the drug to tumor and cancer cell nucleus with minimum non-specific accumulation in heart, which consequently enhanced antitumor activity.

Supplementary Material

Refer to Web version on PubMed Central for supplementary material.

Acknowledgments

This work was supported by R01 CA129287.

References

1. Peer D, Karp JM, Hong S, Farokhzad OC, Margalit R, Langer R. Nanocarriers as an emerging platform for cancer therapy. Nat Nanotechnol. 2007; 2:751–760. [PubMed: 18654426]
2. Wagner V, Dullaart A, Bock A-K, Zweck A. The emerging nanomedicine landscape. Nat Biotechnol. 2006; 24:1211–1217. [PubMed: 17033654]
3. Ferrari M. Cancer nanotechnology: opportunities and challenges. Nat Rev Cancer. 2005; 5:161–171. [PubMed: 15738981]

$watermark-text
$watermark-text
$watermark-text

4. Cabral H, Matsumoto Y, Mizuno K, et al. Accumulation of sub-100 nm polymeric micelles in poorly permeable tumours depends on size. Nat Nanotechnol. 2011; 6:815–823. [PubMed: 22020122]
5. Ashley CE, Carnes EC, Phillips GK, et al. The targeted delivery of multicomponent cargos to cancer cells by nanoporous particle-supported lipid bilayers. Nat Mater. 2011; 10:389–397. [PubMed: 21499315]
6. Von Maltzahn G, Park J-H, Lin KY, et al. Nanoparticles that communicate in vivo to amplify tumour targeting. Nat Mater. 2011; 10:545–552. [PubMed: 21685903]
7. Chauhan VP, Stylianopoulos T, Martin JD, et al. Normalization of tumour blood vessels improves the delivery of nanomedicines in a size-dependent manner. Nat Nanotechnol. 2012; 7:383–388. [PubMed: 22484912]
8. Murphy EA, Majeti BK, Mukthavaram R, Acevedo LM, Barnes LA, Cheresh DA. Targeted Nanogels: A versatile platform for drug delivery to tumors. Mol Cancer Ther. 2011; 10:972–982. [PubMed: 21518727]
9. Xiao K, Luo J, Fowler WL, et al. A self-assembling nanoparticle for paclitaxel delivery in ovarian cancer. Biomaterials. 2009; 30:6006–6016. [PubMed: 19660809]
10. Bae YH, Park K. Targeted drug delivery to tumors: myths, reality and possibility. J Control Release. 2011; 153:198–205. [PubMed: 21663778]
11. Ruenraroengsak P, Cook JM, Florence AT. Nanosystem drug targeting: facing up to complex realities. J Control Release. 2010; 141:265–276. [PubMed: 19895862]
12. Siegwart DJ, Whitehead KA, Nuhn L, et al. Combinatorial synthesis of chemically diverse core-shell nanoparticles for intracellular delivery. Proc Nat Acad Sci USA. 2011; 108:12996–3001. [PubMed: 21784981]
13. Kim JY, Kim S, Pinal R, Park K. Hydrotropic polymer micelles as versatile vehicles for delivery of poorly water-soluble drugs. J Control Release. 2011; 152:13–20. [PubMed: 21352878]
14. Giacomelli C, Schmidt V, Aissou K, Borsali R. Block copolymer systems: from single chain to self-assembled nanostructures. Langmuir. 2010; 26:15734–15744. [PubMed: 20364859]
15. Yamamoto Y, Nagasaki Y, Kato Y, Sugiyama Y, Kataoka K. Long-circulating poly(ethylene glycol)-poly(d,l-lactide) block copolymer micelles with modulated surface charge. J Control Release. 2001; 77:27–38. [PubMed: 11689257]
16. Matsumura Y, Maeda H. A new concept for macromolecular therapeutics in cancer chemotherapy: mechanism of tumoritropic accumulation of proteins and the antitumor agent Smancs. Cancer Res. 1986; 46:6387–6392. [PubMed: 2946403]
17. Savic R, Azzam T, Eisenberg A, Maysinger D. Assessment of the integrity of poly(caprolactone)-b-poly(ethylene oxide) micelles under biological conditions: a fluorogenicbased approach. Langmuir. 2006; 22:3570–578. [PubMed: 16584228]
18. Chen H, Kim S, He W, et al. Fast release of lipophilic agents from circulating PEG-PDLLA micelles revealed by in vivo Forster resonance energy transfer imaging. Langmuir. 2008; 24:5213–5217. [PubMed: 18257595]
19. Letchford K, Burt HM. Copolymer micelles and nanospheres with different in vitro stability demonstrate similar paclitaxel pharmacokinetics. Mol Pharm. 2012; 9:248–260. [PubMed: 22204437]
20. Mitragotri S, Lahann J. Physical approaches to biomaterial design. Nat Mater. 2009; 8:15–23. [PubMed: 19096389]
21. Moghimi SM, Hunter AC, Murray JC. Long-circulating and target-specific nanoparticles: theory to practice. Pharmacol Rev. 2001; 53:283–318. [PubMed: 11356986]
22. Jocelyn, PC. Biochemistry of the SH Group. London: Academic Press; 1972.
23. Sevier CS, Kaiser CA. Formation and transfer of disulphide bonds in living cells. Nat Rev Mol Cell Biol. 2002; 3:836–847. [PubMed: 12415301]
24. Cantin AM, North SL, Hubbard RC, Crystal RG. Normal alveolar epithelial lining fluid contains high levels of glutathione. J Appl Physiol. 1987; 63:152–157. [PubMed: 3040659]
25. Smith CV, Jones DP, Guenthner TM, Lash LH, Lauterburg BH. Compartmentation of glutathione: implications for the study of toxicity and disease. Toxicol Appl Pharmacol. 1996; 140:1–12. [PubMed: 8806864]

$watermark-text

$watermark-text

$watermark-text

26. Russo A, DeGraff W, Friedman N, Mitchell JB. Selective modulation of glutathione levels in human normal versus tumor cells and subsequent differential response to chemotherapy drugs. Cancer Res. 1986; 46:2845–2848. [PubMed: 2421885]
27. Cook JA, Pass HI, Iype SN, et al. Cellular glutathione and thiol measurements from surgically resected human lung tumor and normal lung tissue. Cancer Res. 1991; 51:4287–4294. [PubMed: 1868449]
28. Balendiran GK, Dabur R, Fraser D. The role of glutathione in cancer. Cell Biochem Funct. 2004; 22:343–352. [PubMed: 15386533]
29. Chen H, Kim S, Li L, Wang S, Park K, Cheng J-X. Release of hydrophobic molecules from polymer micelles into cell membranes revealed by Forster resonance energy transfer imaging. Proc Nat Acad Sci USA. 2008; 105:6596–6601. [PubMed: 18445654]
30. Matsumoto J, Nakada Y, Sakurai K, Nakamura T, Takahashi Y. Preparation of nanoparticles consisted of poly(l-lactide)-poly(ethylene glycol)-poly(l-lactide) and their evaluation in vitro. Int J Pharm. 1999; 185:93–101. [PubMed: 10425369]
31. Ahmed F, Discher DE. Self-porating polymersomes of PEG-PLA and PEG-PCL: hydrolysistriggered controlled release vesicles. J Control Release. 2004; 96:37–53. [PubMed: 15063028]
32. Lee S-Y, Lee S, Youn I-C, et al. A near-infrared fluorescence-based optical thermosensor. Chemistry. 2009; 15:6103–6106. [PubMed: 19441001]
33. Choi KY, Yoon HY, Kim J-H, et al. Smart nanocarrier based on PEGylated hyaluronic acid for cancer therapy. ACS Nano. 2011; 5:8591–8599. [PubMed: 21967065]
34. Lovell JF, Jin CS, Huynh E, et al. Porphysome nanovesicles generated by porphyrin bilayers for use as multimodal biophotonic contrast agents. Nat Mater. 2011; 10:324–332. [PubMed: 21423187]
35. Schlessinger J, Axelrod D, Koppel D, Webb W, Elson E. Lateral transport of a lipid probe and labeled proteins on a cell membrane. Science. 1977; 195:307–309. [PubMed: 556653]
36. Li Y, Song Y, Zhao L, Gaidosh G, Laties AM, Wen R. Direct labeling and visualization of blood vessels with lipophilic carbocyanine dye DiI. Nat Protoc. 2008; 3:1703–1708. [PubMed: 18846097]
37. Axelrod D. Carbocyanine dye orientation in red cell membrane studied by microscopic fluorescence polarization. Biophys J. 1979; 26:557–573. [PubMed: 263688]
38. Wooles WR, Di Luzio NR. Reticuloendothelial function and the immune response. Science. 1963; 142:1078–1080. [PubMed: 14068228]
39. Singal PK, Iliskovic N. Doxorubicin-induced cardiomyopathy. N Engl J Med. 1998; 339:900–905. [PubMed: 9744975]
40. Andrew MacKay J, Chen M, McDaniel JR, Liu W, Simnick AJ, Chilkoti A. Self-assembling chimeric polypeptide-doxorubicin conjugate nanoparticles that abolish tumours after a single injection. Nat Mater. 2009; 8:993–999. [PubMed: 19898461]
41. Yamada A, Taniguchi Y, Kawano K, Honda T, Hattori Y, Maitani Y. Design of folate-linked liposomal doxorubicin to its antitumor effect in mice. Clin Cancer Res. 2008; 14:8161–8168. [PubMed: 19088031]
42. Taniguchi Y, Kawano K, Minowa T, Sugino T, Shimojo Y, Maitani Y. Enhanced antitumor efficacy of folate-linked liposomal doxorubicin with TGF-β type I receptor inhibitor. Cancer Sci. 2010; 101:2207–2213. [PubMed: 20608940]
43. Ko JY, Park S, Lee H, et al. pH-sensitive nanoflash for tumoral acidic pH imaging in live animals. Small. 2010; 6:2539–2544. [PubMed: 20979241]
44. Murakami M, Cabral H, Matsumoto Y, et al. Improving drug potency and efficacy by nanocarrier-mediated subcellular targeting. Sci Transl Med. 2011; 3:64ra2.
45. Werner ME, Copp JA, Karve S, et al. Folate-targeted polymeric nanoparticle formulation of docetaxel is an effective molecularly targeted radiosensitizer with efficacy dependent on the timing of radiotherapy. ACS Nano. 2011; 5:8990–8998. [PubMed: 22011071]
46. Koo AN, Min KH, Lee HJ, et al. Tumor accumulation and antitumor efficacy of docetaxelloaded core-shell-corona micelles with shell-specific redox-responsive cross-links. Biomaterials. 2012; 33:1489–1499. [PubMed: 22130564]

47. Li Y, Xiao K, Luo J, et al. Well-defined, reversible disulfide cross-linked micelles for ondemand paclitaxel delivery. Biomaterials. 2011; 32:6633–6645. [PubMed: 21658763]
48. Byrne JD, Betancourt T, Brannon-Peppas L. Active targeting schemes for nanoparticle systems in cancer therapeutics. Adv Drug Deliv Rev. 2008; 60:1615–1626. [PubMed: 18840489]
49. Kirpotin DB, Drummond DC, Shao Y, et al. Antibody targeting of long-circulating lipidic nanoparticles does not increase tumor localization but does increase internalization in animal models. Cancer Res. 2006; 66:6732–6740. [PubMed: 16818648]
50. Bartlett DW, Su H, Hildebrandt IJ, Weber WA, Davis ME. Impact of tumor-specific targeting on the biodistribution and efficacy of siRNA nanoparticles measured by multimodality in vivo imaging. Proc Nat Acad Sci USA. 2007; 104:15549–15554. [PubMed: 17875985]

$watermark-text
$watermark-text
$watermark-text

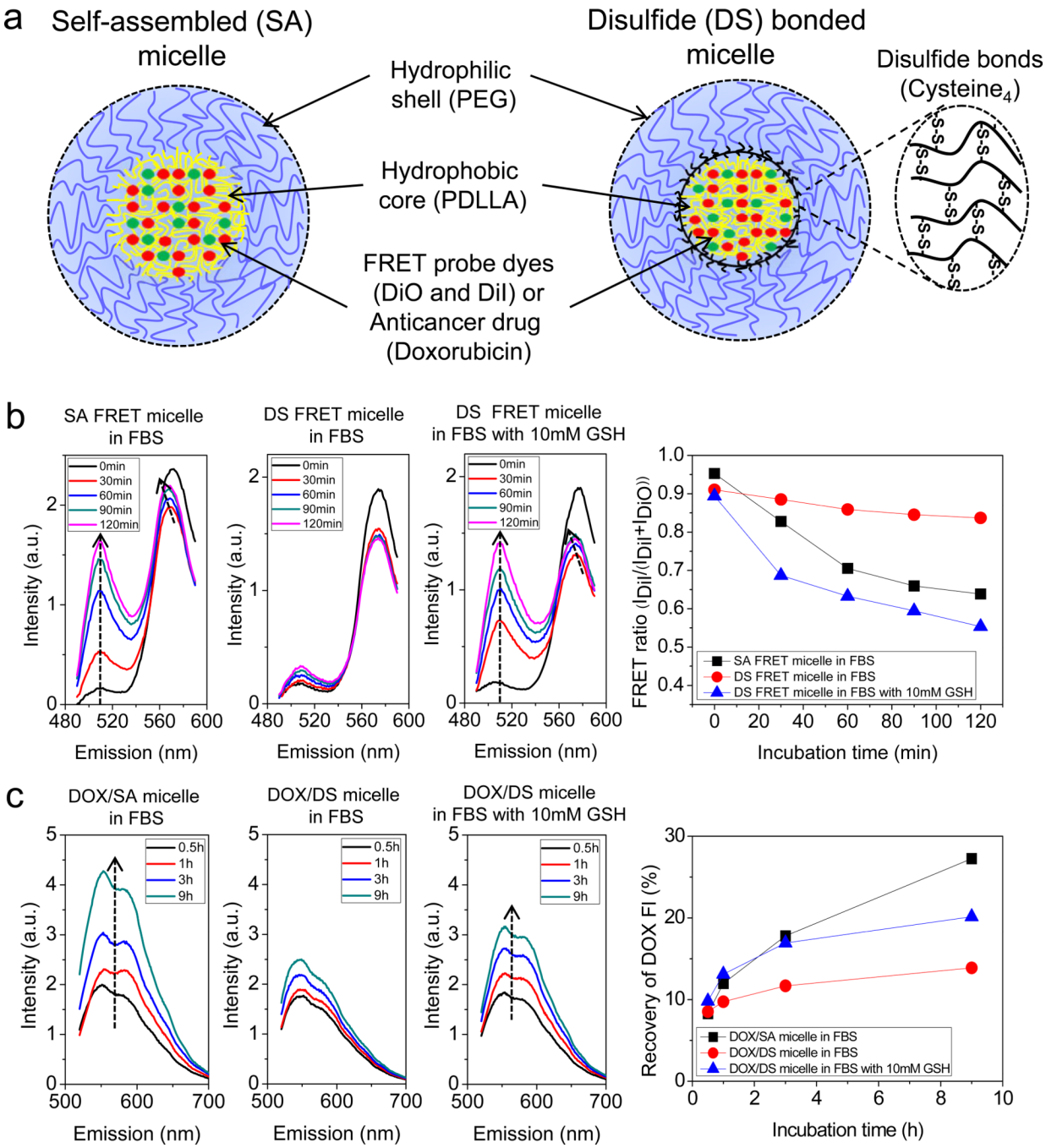

Fig. 1.

Higher stability and reducibility of disulfide (DS) bonded micelles in serum, confirmed using FRET and the self-quenching properties of DOX. (a) Schematic illustrations of self-assembled (SA) and disulfide (DS) bonded micelles with FRET dyes (DiO and DiI) or doxorubicin (DOX). (b) Time-resolved spectra of SA and DS FRET micelles in 80% (v/v) FBS without or with 10 mM GSH at 37°C. FRET ratio, $I_{DiI}/(I_{DiI}+I_{DiO})$, as a function of incubation time. I_{DiI} and I_{DiO} represent the fluorescence intensities of DiI at 570 nm and DiO at 508 nm in the spectrum measurements. (c) Time-lapse spectra of DOX/SA and DOX/DS micelles in 80% (v/v) FBS without or with 10 mM GSH at 37°C. Recovery of DOX fluorescence intensity, $((F-F_W)/F_D)\times100$, as a function of incubation time. FW and FD

$watermark-text
$watermark-text
$watermark-text

correspond to the integrated fluorescence for the micelles in water and DMSO with 100 mM DTT.

$watermark-text

$watermark-text

$watermark-text

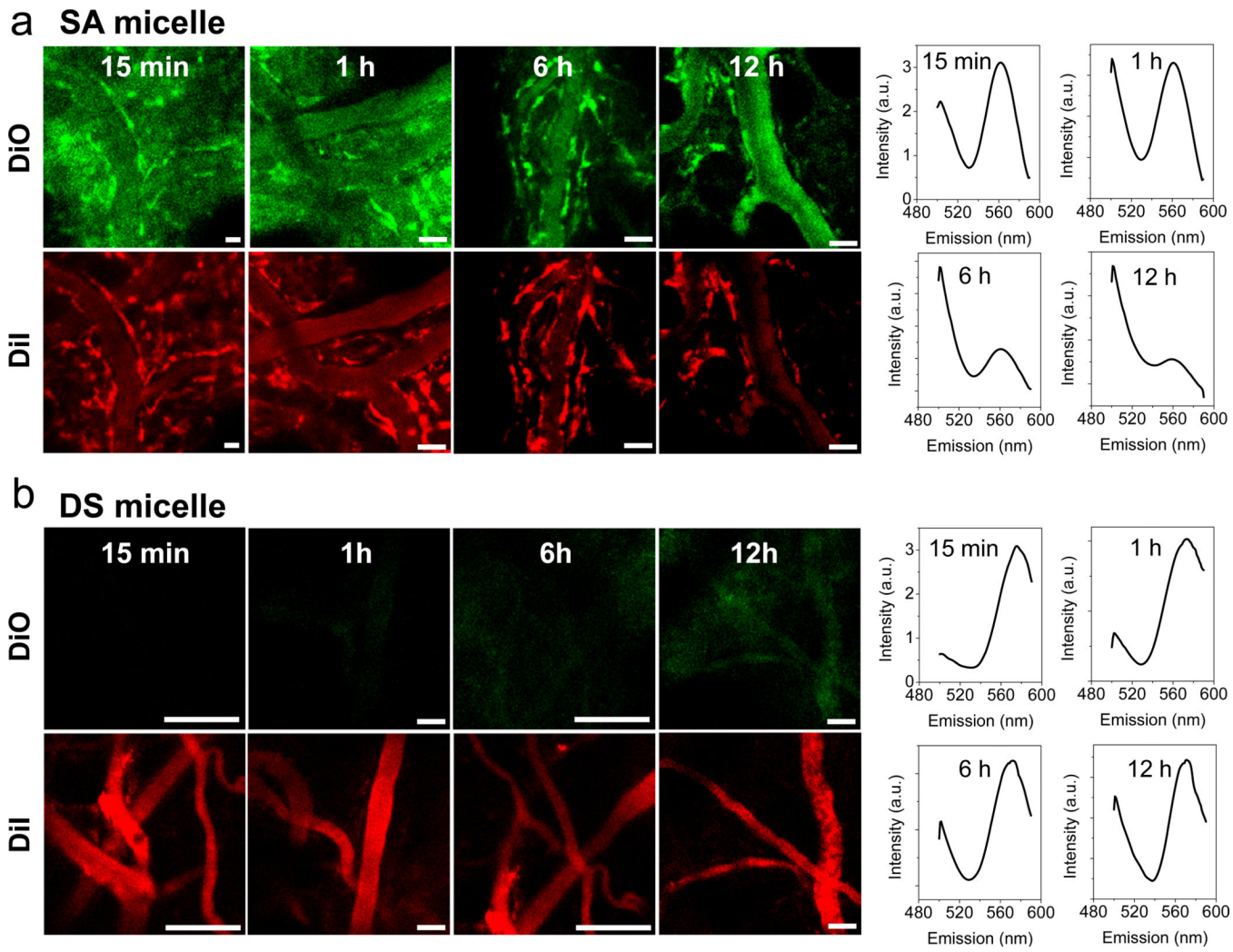

Fig. 2.

Unbroken DS micelles during blood circulation. *In vivo* real-time FRET imaging of blood vessels in mouse ears after i.v. injection of (a) SA or (b) DS FRET micelles. The green and red colors represent DiO and DiI signals (Scale bar: 40 μm). Fluorescence spectra (right) of FRET micelles in the blood vessels were measured at different time points. The excitation was 488 nm.

$watermark-text
$watermark-text
$watermark-text

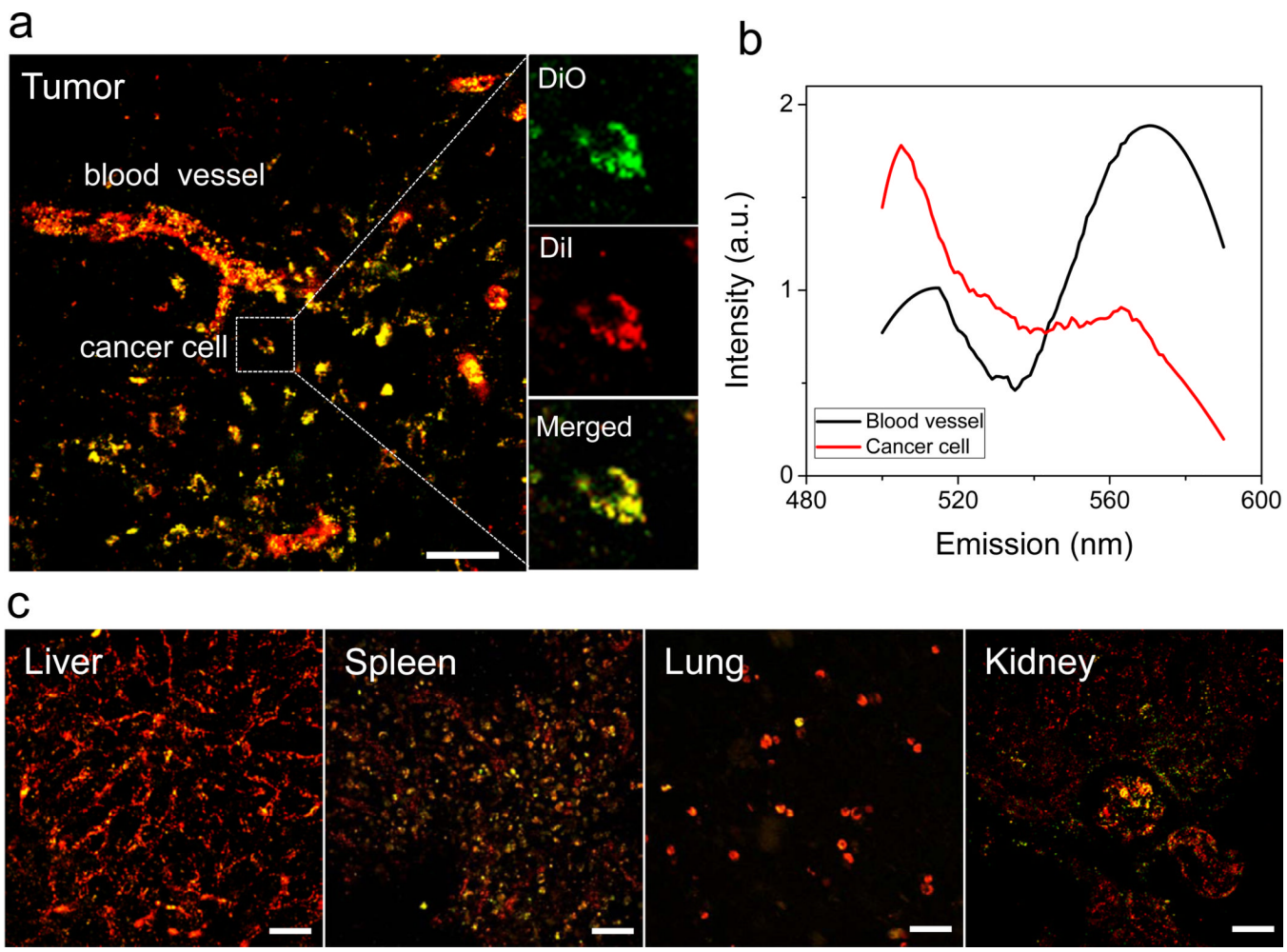

Fig. 3.

Adapted DS micelles in tumor. (a) Confocal FRET image of M109 tumor tissue at 6 h after i.v. injection of DS FRET micelles. The figure is the merged image of DiO (green) and DiI (red) channels. The yellow color indicates overlapped signals from both FRET dyes. (Scale bar: 40 μm). High-magnification image (right image) of a single cancer cell with DiO (green), DiI (red), and merged channels are shown. (b) Fluorescence spectra of DS FRET micelles in blood vessel and cancer cell were measured. (c) FRET images of other tissues (liver, spleen, lung, and kidney). (Scale bar: 40 μm).

$watermark-text
$watermark-text
$watermark-text

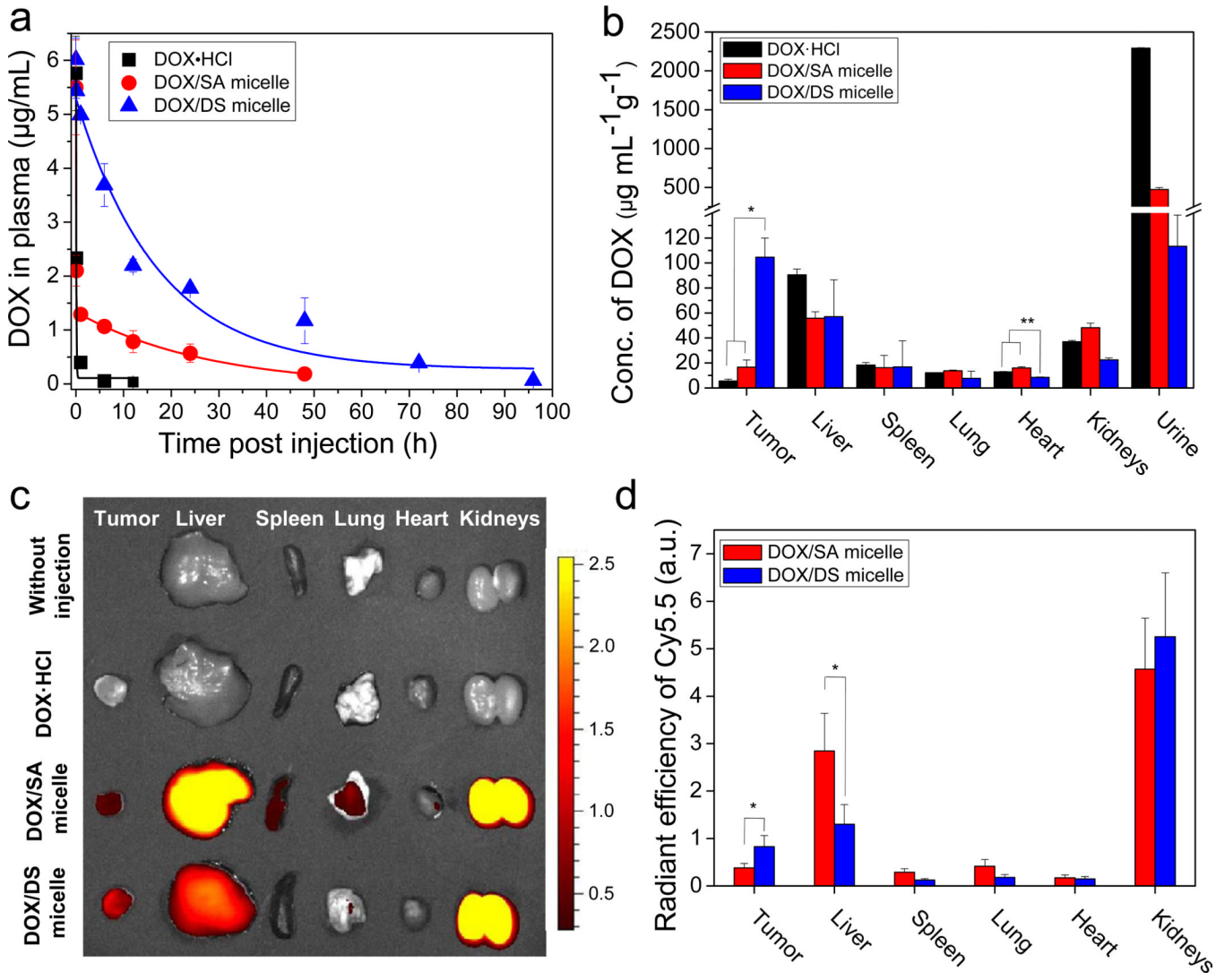

Fig. 4.

Prolonged blood retention time and improved tumor-targeting efficacy of DOX via DS micelles. (a) Blood retention kinetics of DOX·HCl, DOX loaded in SA and DS micelles in mice. DOX·HCl (at 4 mg/kg), DOX/SA and DOX/DS micelles (at 4 mg DOX equiv/kg) were intravenously injected. The data were fitted with a one-compartment model ($y = Ae^{(-x/t)} + y_0$) for DOX·HCl and DOX/DS micelle groups or a two-compartment model ($y = A_1e^{(-x/t1)} + A_2e^{(-x/t2)} + y_0$) for DOX/SA micelle group. Data are expressed as means ± SEM (n=5). (b) Tissue distribution of DOX at 1 day-post injection. DOX·HCl (at 4 mg/kg), DOX/SA(-Cy5.5) and DOX/DS(-Cy5.5) micelles (at 4 mg DOX equiv/kg, with similar absorption intensity of Cy5.5) were intravenously injected to M109 bearing mice. means ± SEM (n=4). *$P < 0.005$; **$P < 0.001$. (c) Fluorescent image of tissue distribution of Cy5.5-labeled SA and DS micelles at 1 day-post injection. (d) Quantitative analysis of Cy5.5-labeled SA and DS micelles in tissues. Values are means ± SEM (n=4). *$P < 0.05$

$watermark-text
$watermark-text
$watermark-text

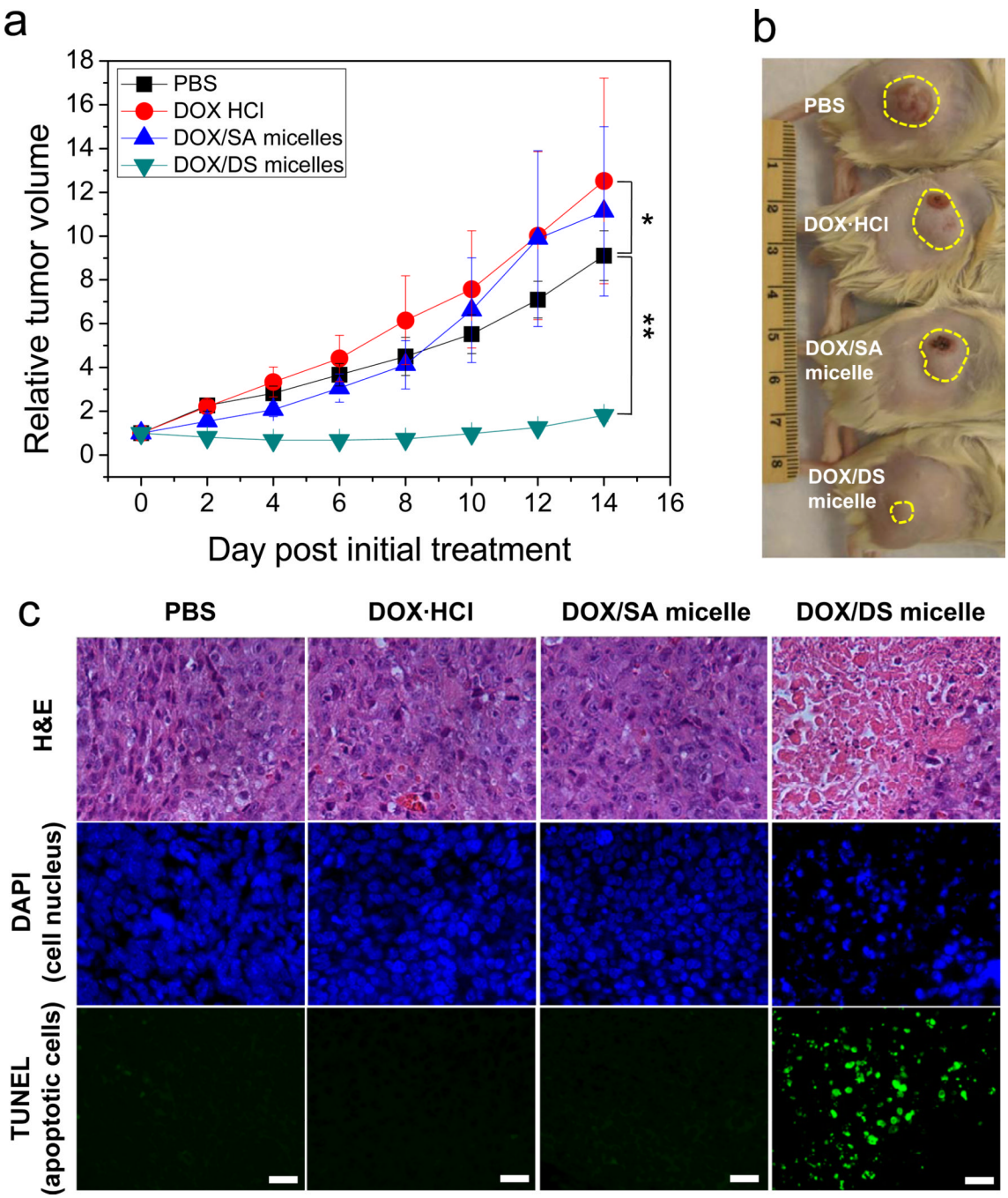

Fig. 5.

Enhanced antitumor effects of DOX via DS micelles. (a) Relative tumor volume (the ratio of tumor volume to initial size before treatment) for M109 tumor as a function of time. DOX·HCl (2 mg/kg), DOX/SA, and DOX/DS micelles (2 mg DOX Equiv/kg) were intravenously injected at Day 0 and 4. Data are expressed as means ± SEM (n=6~8). $*P > 0.1$; $**P < 0.005$. (b) Photograph showing representative tumor size in each group at 14 days after initial treatment. The yellow dotted circle indicates the M109 solid tumor. (c) Apoptotic M109 cancer cells stained by TUNEL immunohistochemistry. Fluorescence blue and green indicate DAPI (cell nucleus) and TUNEL (apoptotic cells) signals, respectively. (Scale bar: 40 μm).

$watermark-text
$watermark-text
$watermark-text

$watermark-text
$watermark-text
$watermark-text

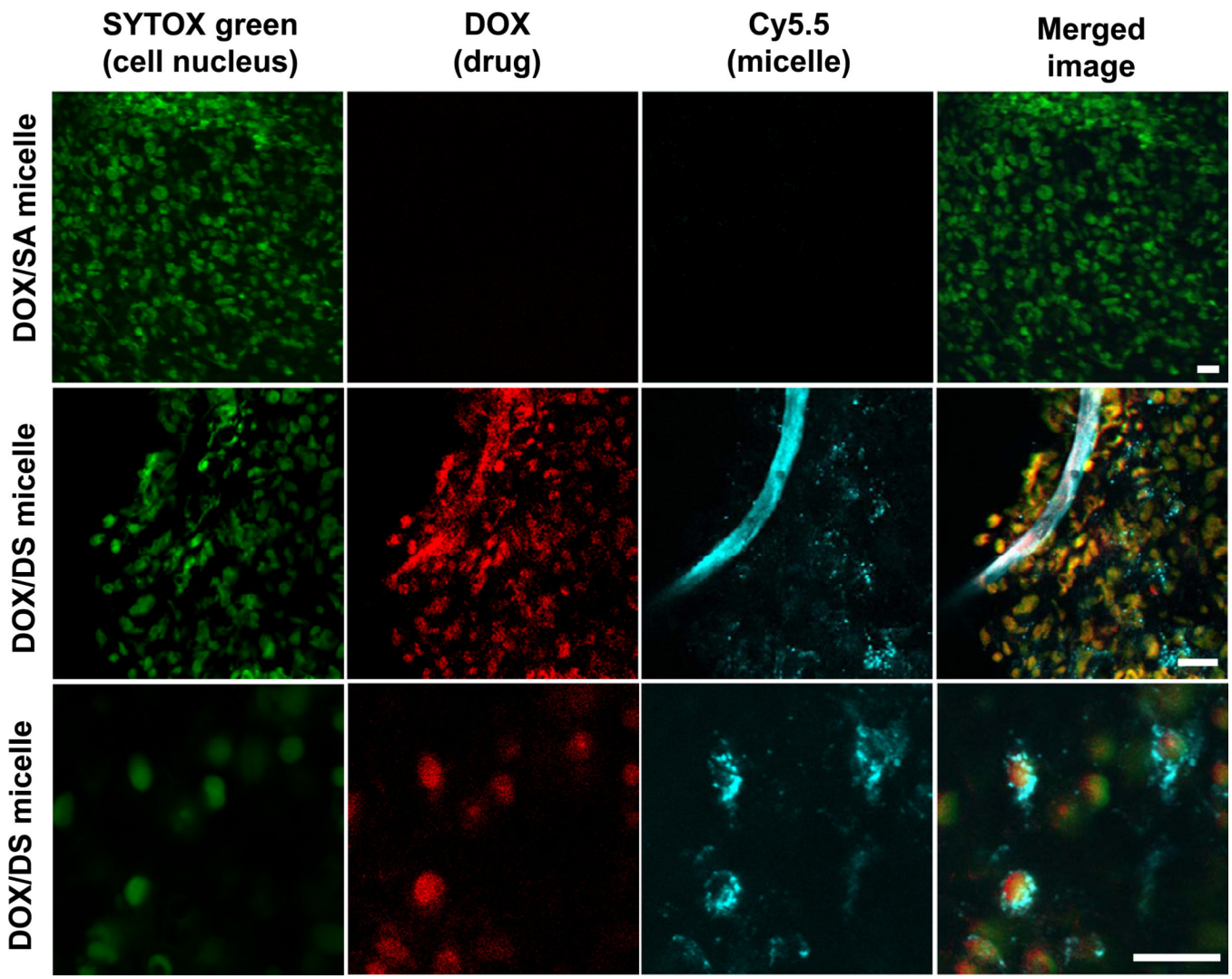

Fig. 6.

Nuclear delivery of DOX via DS micelles. Confocal fluorescence images of cancer cells in tumor tissues at 12 h after i.v. injection of DOX/SA(-Cy5.5) or DOX/DS(-Cy5.5) to M109 bearing mice. Fluorescence green, red, and cyan blue indicate SYTOX (cell nucleus), DOX (anti-cancer drug), and Cy5.5 (micelle) signals, respectively. Yellow and white colors represent the overlapping signals of DOX with SYTOX and Cy5.5. (Scale bar: 20 μm).